COLLEGE OF ENGINEERING

VIRGINIA POLYTECHNIC INSTITUTE AND STATE UNIVERSITY

BLACKSBURG, VIRGINIA

College of Engineering
Virginia Polytechnic Institute and State University
Blacksburg, VA 24061

VPI-E-76-21 September 1976

STRESS-STRAIN AND FAILURE PROPERTIES OF GRAPHITE/ EPOXY LAMINATES

Y. T. Yeow, Research Associate
H. F. Brinson, Professor

Department of Engineering Science and Mechanics

Prepared for:

National Aeronautics and Space Administration
Grant No. NASA-NSG 2038
Materials Science Branch
Ames Research Center
Moffett Field, CA 94035

BIBLIOGRAPHIC DATA SHEET	1. Report No. VPI-E-76-21	2.	3. Recipient's Accession No.

4. Title and Subtitle

STRESS-STRAIN AND FAILURE PROPERTIES OF GRAPHITE/EPOXY LAMINATES

5. Report Date Sept. 1976

6.

7. Author(s)

Y. T. Yeow, H. F. Brinson

8. Performing Organization Rept. No.

9. Performing Organization Name and Address

Engineering Science and Mechanics
Virginia Polytechnic Inst. & State University
Blacksburg, VA 24061

10. Project/Task/Work Unit No.

11. Contract/Grant No.

NASA-NSG-2038

12. Sponsoring Organization Name and Address

NASA
Materials Science Branch
Ames Research Center
Moffett Field, CA 94035

13. Type of Report & Period Covered

Sept. 1976

14.

15. Supplementary Notes

16. Abstracts

The results of a series of tensile tests on graphite/epoxy $[0°]_{8S}$ and $[0°/\pm 30°/0°]_{2S}$ laminates at rates varying from 0.002 in/min to 2 in/min are reported. The loads are applied at various angles to the fiber directions in each case. The rate dependent behavior of the stress-strain response is assessed. Evidence is presented to indicate that failure first occurs on inner plies. Also, evidence is presented to indicate that, in some cases, moduli increase with increased stress or strain level. Lamination theory is used to predict moduli and comparisons with experiment are given. Also, lamination theory is used in conjunction with three failure theories to predict ultimate strengths with varying degrees of success.

17. Key Words and Document Analysis. 17a. Descriptors

composites, failure, stress-strain response

17b. Identifiers/Open-Ended Terms

17c. COSATI Field/Group

18. Availability Statement	19. Security Class (This Report)	21. No. of Pages
Distribution Unlimited	UNCLASSIFIED	35
	20. Security Class (This Page) UNCLASSIFIED	22. Price

STRESS-STRAIN AND FAILURE PROPERTIES OF GRAPHITE/EPOXY LAMINATES

ABSTRACT

The results of a series of tensile tests on graphite/epoxy $[0°]_{8S}$ and $[0°/\pm 30°/0°]_{2S}$ laminates at rates varying from 0.002 in/min to 2 in/min are reported. The loads are applied at various angles to the fiber directions in each case. The rate dependent behavior of the stress-strain response is assessed. Evidence is presented to indicate that failure first occurs on inner plies. Also, evidence is presented to indicate that, in some cases, moduli increase with increased stress or strain level. Lamination theory is used to predict moduli and comparisons with experiment are given. Also, lamination theory is used in conjunction with three failure theories to predict ultimate strengths with varying degrees of success.

Introduction

The proper characterization of advanced laminated composite materials is quite complex due to their inhomogeneous and anisotropic nature and due to the coupling effects caused by the lamination process. The latter often results in delaminations or stacking sequence effects as shown by Daniel, et al.[1] Numerous testing techniques[2] and analytical techniques[3] have been proposed for the characterization of composite materials. Basically, the behavior of composites can be assessed from a micromechanical or a macromechanical viewpoint. Essentially, the rule of mixtures is representative of the former approach and lamination theory is representative of the latter.

The macroscopic approach of lamination theory has been used in the present effort. In brief, the goal of this study was to investigate the tensile properties of $[0°]_{8S}$ and $[0°/\pm30°/0°]_{2S}$ graphite/epoxy laminates. This included moduli and strengths and their prediction by appropriately applying lamination theory in conjunction with several failure theories. Further, the viscoelastic or rate dependent behavior of the laminates investigated (Hercules AS fiber and 3501 resin) was to be determined.

Analytical Considerations

The constitutive relations using classical lamination theory for an orthotropic lamina in a state of plane stress can be written as[4]

$$\begin{Bmatrix} \sigma_1 \\ \sigma_2 \\ \tau_{12} \end{Bmatrix}^K = \begin{bmatrix} C_{11} & C_{12} & 0 \\ C_{12} & C_{22} & 0 \\ 0 & 0 & C_{66} \end{bmatrix} \begin{Bmatrix} \varepsilon_1 \\ \varepsilon_2 \\ \gamma_{12} \end{Bmatrix}^K \qquad (1)$$

The C_{ij} are the stiffnesses and K refers to the K^{th} lamina. Only four elastic constants are required, namely, E_{11}, E_{22}, G_{12} and ν_{12} where the subscripts 1 and 2 refer to the fiber direction and transverse to the fiber direction respectively. The latter constants are related to the stiffnesses (C_{ij}).[3,4] The 1-2 coordinate system is along the axes of material symmetry. This local coordinate system can be transformed into the global laminate x-y coordinate system which gives the following constitutive relations for a lamina

$$\begin{Bmatrix} \sigma_x \\ \sigma_y \\ \tau_{xy} \end{Bmatrix}^K = \begin{bmatrix} \bar{C}_{11} & \bar{C}_{12} & \bar{C}_{16} \\ \bar{C}_{12} & \bar{C}_{22} & \bar{C}_{26} \\ \bar{C}_{16} & \bar{C}_{26} & \bar{C}_{66} \end{bmatrix}^K \begin{Bmatrix} \varepsilon_x \\ \varepsilon_y \\ \gamma_{xy} \end{Bmatrix}^K \tag{2}$$

Here the $\bar{C}_{ij}$ are the transformed or reduced stiffnesses.

The laminate stiffnesses, A_{ij}, can be calculated from the transformed laminae stiffnesses, $\bar{C}_{ij}$.[3] For a symmetric laminate, the in-plane loads are related to the in-plane laminate strains, $\{\varepsilon_j^\circ\}$, by

$$\{N_i\} = [A_{ij}]\ \{\varepsilon_j{}^\circ\}, \qquad i \text{ and } j = x \text{ or } y \tag{3}$$

where $\{N_i\}$ are the resultant forces per unit length of the laminate. (For uniaxial tension $N_x \neq 0$ and $N_y = N_{xy} = 0$.) Thus, the in-plane strains can be calculated knowing the in-plane laminate stress resultants and the properties of a single lamina. Further, this information can be used to calculate the stresses in any layer or lamina in terms of the externally applied loads. Since interlaminar effects are not included, the analysis predicts identical response for a given laminate regardless of stacking sequence of individual plys.

Numerous failure criteria are presently available[5] which can be classified as either having independent or dependent failure modes. The maximum stress or maximum strain criterion are ones with independent failure modes. The criteria proposed by Ashkenazi,[6] Hill[7] and Puppo and Evensen[8] are examples of failure theories with dependent failure modes. Between the two classes, it would seem that those with dependent failure modes would be more appropriate for composite materials. Experimental results tend to confirm this assumption.[9]

Ashkenazi's theory assumes a macroscopic continuum in which the strength properties are fourth order tensors and in which environmental effects are neglected. His criterion for a plane orthotropic material under uniaxial load in an arbitrary direction is

$$\frac{1}{\sigma_x} = \frac{\cos^4\theta}{X} + \left(\frac{4}{X_{45}} - \frac{1}{X} - \frac{1}{Y}\right)\sin^2\theta\,\cos^2\theta + \frac{\sin^4\theta}{Y} \qquad (4)$$

where σ_x is the applied normal stress making an angle θ with the principal material direction (1 or fiber direction) and X, Y and X_{45} are the tensile strengths along, transverse to and at 45° to the principal material direction respectively. While equation (4) is for uniaxial loading only, other stress states are considered by the author.

Using assumptions similar to those of Ashkenazi, Hill developed the failure criterion for an orthotropic material under a generalized state of plane stress

$$\left(\frac{\sigma_1}{X}\right)^2 + \left(\frac{\sigma_2}{Y}\right)^2 - \frac{\sigma_1\sigma_2}{XY} + \left(\frac{\tau_{12}}{S}\right)^2 = 1 \qquad (5)$$

where the stresses $\sigma_1 \sigma_2$, τ_{12} are along the material axes, S is the in-plane shear strength and X and Y are as previously defined.

A more general theory due to Puppo and Evensen can be expressed as

$$\left(\frac{\sigma 1}{X}\right)^2 - \gamma\left(\frac{X}{Y}\right)\left(\frac{\sigma 1}{X}\right)\left(\frac{\sigma 2}{Y}\right) + \gamma\left(\frac{\sigma 2}{Y}\right)^2 + \left(\frac{\tau 12}{S}\right)^2 = 1$$

$$\gamma\left(\frac{\sigma 1}{X}\right)^2 - \gamma\left(\frac{Y}{X}\right)\left(\frac{\sigma 1}{X}\right)\left(\frac{\sigma 2}{Y}\right) + \left(\frac{\sigma 2}{Y}\right)^2 + \left(\frac{\tau 12}{S}\right)^2 = 1 \qquad (6)$$

where $\gamma = \frac{3S^2}{XY}$ is an interaction factor and the other quantities are as previously defined. Further, the authors indicated that their theory could be adapted to a wide range of materials by writing the interaction factor as $\gamma = \left(\frac{3S^2}{XY}\right)^n$. Equations (6) are for orthotropic materials but the general theory is not so limited.

The failure theories given above are used in connection with lamination theory in the following way. The properties of a single ply or lamina must first be determined. As single plies are quite thin, $\sim$ 0.005 in, (0.127 mm), properties are usually determined by testing a multi-layered unidirectional laminate. These are taken as the assumed properties of a single ply and the properties, A_{ij}, of general laminates are then calculated for each configuration being considered. (Obviously, if the properties of the unidirectional laminate do not represent the properties of a single ply or if different defects are present in the manufacture of the general laminate as opposed to the unidirectional laminate, the "calculated" properties are likely to be in error.) From a knowledge of the experimental loads and the A_{ij}, the in-plane strains, $\overset{\circ}{\varepsilon}_j$, can be

calculated from equation (3). These can be used to determine stress, σ_i, in the K^{th} layer from equation (2) which can then be substituted into the appropriate failure criteria. Thus, each failure theory is then expressed in terms of the applied loads N_i and a general laminate can be examined ply-wise for each load increment until a lamina reaches the failure state. (σ_i and N_i above refer in each case to global coordinates.)

The difficult question encountered after first ply failure (FPF)[10] is how unloading occurs. Petite and Waddoups[11] use the negative tangent modulus technique to unload the failed ply together with a maximum strain concept to uncouple lamina stiffnesses. An alternate approach due to Sandhu[12] is similar except it uses a maximum strain energy concept to uncouple the failed lamina. Another simple technique cited by Jones[3] is to uncouple the degraded lamina by assigning zero stiffnesses to the three off-diagonal terms of equations (2). The appropriate diagonal terms are zeroed using a maximum strain criteria when and if a diagonal strain is exceeded.

We have elected to use a different approach to account for the reduced laminate load carrying capacity due to FPF. In any general laminate certain plies are likely to fail first. For example in a $[0°/\pm30°/0°]_S$ tested in uniaxial tension in the 0°, FPF likely occurs in one of the ± 30° plies. Each such ply would not necessarily fail at the same time or have the same failure plane. It is assumed, however, that failure in each 30° ply would occur simultaneously but planes would be staggered as shown in Fig. 1a. Final failure is assumed to occur as shown in Fig. 1b. The analysis procedure of this staggered FPF model follows.

Using lamination theory and any of the previously mentioned failure criteria, the laminate is loaded incrementally until FPF occurs (e.g., the 30° plies for a $[0°/\pm30°/0°]_S$ as shown in Fig. 1a). The remote stress for uniaxial tension of a laminate prior to FPF is given as

$$\sigma_n = \frac{P}{WT} \tag{7}$$

where P, W and T are the applied load and the laminate width and thickness respectively. After FPF, the stiffnesses of the failed laminae (± 30°) are zeroed and the remote stress is taken to be

$$\sigma_n = \frac{P}{WT'} \tag{8}$$

where T' is the new assumed laminate thickness. For the $[0°/\pm30°/0°]_S$ example of Fig. 1a, T = 8t and T' = 6t where t is the lamina thickness. Note that the new thickness T' = 6t assumes that the "failed" ± 30° plies are still capable of carrying a fraction of the applied stress and are not assumed to be completely ineffective. The laminate continues to carry load until final fracture as shown in Fig. 1b.

The procedure described above can be used for any laminate. Of course, for a unidirectional laminate, FPF is equivalent to total failure. Because interlaminar stresses are neglected this approach gives slightly conservative results for general laminates as will later be demonstrated.

Nonlinear lamina material behavior is easily incorporated in laminate failure predictions due to the incremental nature of the computational procedure. In addition, the procedure can be used to predict

the uniaxial stress-strain response of a laminate for the same reason.

Experimental Procedures and Results

The materials studied in this investigation were manufactured by Lockheed (Sunnyvale, Calif.) from prepreg tapes composed of Hercules (Magna, Utah) graphite AS fibers and epoxy resin 3501. The fundamental properties of the fibers were: 380-400 ksi (~ 2620-2760 MPa) tensile strength, 30-40 x 10^3 ksi (~ 207-276 MPa) elastic modulus and 10,000 fibers/tow. The resin was a hot-melt 100% solids epoxy. No properties of the resin were available. The laminae were about 65% fiber by volume. The resulting $[0°]_{8S}$ and $[0°/\pm30°/0°]_{2S}$ laminates were medium strength-medium modulus composite materials. Large 0.80 in (20.32 mm) thick plates were received from which individual specimens were machined.

Machined surfaces were examined by a scanning electron microscope (SEM) and various inherent flaws were found. Figure 2 shows two such flaws which gives an indication of the size of those found.

Specimens of dimensions 8 in x 0.5 in x 0.08 in (203.2 mm x 12.7 mm x 2.032 mm) were cut from both the $[0°]_{8S}$ and $[0°/\pm30°/0°]_{2S}$ panels with three different orientations. These were in the principal (0°) fiber direction, at 45° to the principal fiber direction and at 90° to the principal fiber direction. After machining, all specimens were stored in a dessiccator until tested. Specimens were allowed to sit and stabilize to the test environment for at least 1 hr prior to testing. Test temperatures were generally at room temperature of approximately 75°F and the relative humidity was generally less than 60%. The specimens were instrumented with longitudinal and transverse strain gages and were

tested in uniaxial tension at strain (head) rates from 0.002 in/min (0.0508 mm/min) to 2 in/min (50.8 mm/min). Both $[0°]_{8S}$ and $[0°/\pm30°/0°]$ laminates were tested at the various rates and with loads at 0°, 45°, and 90° to the principal material direction. All tests were conducted without tabs, using sandpaper between epoxy coated wedge grips to minimize penetration of grip serrations into the graphite/epoxy materials. Data collected in this manner correlated well with data collected by NASA-Ames using tabs.

Because of the variability of stress-strain data, a statistical subroutine from the library of our IBM-370 computer was used to condition the data. Axial loads and longitudinal and transverse strains were fed into the computer program. The program calculated the axial stress, fitted the stress-strain data with a polynomial equation using a technique similar to the least squares method, gave a listing of the polynomial coefficients and plotted the experimental data together with the fitted curve. Most data could be fitted well with a third order polynomial and only a few required a fourth order curve for a good fit. The gradient of the various stress-strain (σ_x - ε_x) or strain-strain (ε_x - ε_y) polynomials at any point was taken as the instantaneous laminate modulus or Poisson's ratio respectively. These instantaneous values for the unidirectional laminate were used as input to lamination theory to obtain the response of the general laminates.

Generally, the instantaneous modulus, $d\sigma/d\varepsilon = E_t$, and Poisson's ratio changed throughout each test by as much as 25%. While decreases usually occurred, increases were noted for the $[0°]_{8S}$ and $[0°/\pm30°/0°]_{2S}$ tests.

Final fracture surfaces were in general perpendicular to the load direction for the $[0°]_{8S}$ and $[0°/\pm30°/0°]_{2S}$ test as is shown in Figure 3. As may be seen from the same figure, longitudinal splitting was always at least a secondary (and sometimes a primary) fracture mode for the $[0°]_{8S}$ tests. All other fracture surfaces for other fiber orientations tended to follow the principal fiber direction.

The fracture process for the $[0°/\pm30°/0°]_{2S}$ specimens was often quite explosive and in many cases fragmentation occurred; i.e., fragments would be expelled considerable distances from the test machine. Also, for this series of tests, post specimen examination did reveal some evidence of delamination. However, it is felt that this delamination occurred after separation due to rebound impact forces (see Figure 3 which shows a specimen which fractured in two places simultaneously).

In many tests various factors indicated that fracture of inner plies occurred first. Figure 4a is an SEM photograph of the central portion of a $[0°]_{8S}$ specimen fracture surface and figure 4b is an SEM photograph of individual broken and pulled out fibers.

For the $[0°/\pm30°/0°]_{2S}$, $[45°/15°/75°/45°]_{2S}$, and $[90°/\pm60°/90°]_{2S}$ tests audible noise could be heard in nearly every case long before separation. Undoubtedly this audible noise was due to breakage of either individual fibers or individual plies and most likely was due to the latter.

Another indication that fracture occurred on inner plies first can be seen by examination of Figure 5 which shows the load-time and strain-time traces from one strain-rate test for a $[90°/\pm60°/90°]_{2S}$ specimen. As may be observed, small excursions in load occurred simultaneously with large excursions in strain. This was accompanied by large amounts of

audible noise with no visible signs of failure on the surface of the specimen. A possible explanation for these observations is that fracture may have occurred first on an inner ply or plies near the location of the strain gage on a surface ply resulting in a transfer of strain from inner to outer plies with little loss in load carrying capacity. Such a porcess could cause a large increase in strain on an outer ply at the strain gage site and not affect the load carrying capacity appreciably.

It should be noted that the manufacturer's specification for the tensile strength of the $[0°]_{8S}$ material was 240 ksi ($\sim$ 1650 MPa). Our tests, substantiated by NASA-Ames, indicated a tensile strength of only 153 ksi ($\sim$ 1050 MPa). This extreme difference seems to be a fault of the manufacturing technique. Also, these graphite/epoxy panels contained extreme thickness variations, i.e., as much as 35%. Thickness variations of individual specimens were considerably less, i.e., $\sim < 10\%$. Such variations in strength and thicknesses are obviously very important in attempts to understand the failure and fracture behavior of composite materials.

Figures 6 through 11 show the stress-strain curves obtained for the $[0°]_{8S}$, $[45°]_{8S}$, $[90°]_{8S}$, $[0°/\pm30°/0°]_{2S}$, $[45°/15°/75°/45°]_{2S}$ and $[90°/\pm60°/90°]_{2S}$ axial tension specimens at the various head rates indicated. Each stress-strain curve was obtained by computer aided statistical conditioning of three separate sets of tension test data for each configuration tested as discussed briefly in the last section. Several interesting facts can be discerned from an examination of Figures 6-11. The curves for the $[0°]_{8S}$ and $[0°/\pm30°/0°]_{2S}$ laminates of Figures 6 and 9 indicate very little rate effect. The differences noted in these

figures were probably due to experimental scatter. When none of the fibers were in the load direction varying degrees of rate effects were apparently present. Figures 7 and 10 tend to indicate that the $[45°]_{8S}$ and $[45°/15°/75°/45°]_{2S}$ materials first show an increase of properties with increasing rate, 0.002 in/min (0.0508 mm/min) and 0.02 in/min (0.508 mm/min) followed by a decrease of properties with increasing rate, 0.2 in/min (5.08 mm/min) and 2.0 in/min (50.8 mm/min). The $[90°/\pm60°/90°]_{2S}$ data of Figure 11 tend to show that properties essentially decrease with increasing rate. Examination of Figure 8 for the $[90°]_{8S}$ laminate indicates, as expected, that when a laminate was matrix dominated properties in fact increased with increasing rate. Apparently some type of transition from a fiber dominated laminate with no rate effect to a matrix dominated laminate with rate effect did exist. The exact form of the transition is unclear but it does appear that if more than 50% of the fibers were in the load direction little rate effect was present. Further, it would seem that for certain stacking sequences, i.e., $[45°]_{2S}$, $[45°/75°/15°/45°]_{2S}$ and $[90°/\pm60°/90°]_{2S}$ that increased rate had a deleterious effect on the material properties.

Bilinearity is evident in Figures 6 and 9 for the $[0°]_{8S}$ and $[0°/\pm30°/0°]_{2S}$ material where the stiffness tends to increase with stress or strain level. This is likely due to the scissoring effect of straightening the fibers or possibly the failure of the 30° plies in the $[0°/\pm30°/0°]_{2S}$ case. Analytical predictions to be discussed tend to confirm this latter observation. Inelastic stress-strain behavior was observed for the other orientations tested. Another interesting fact found was that Poisson's ratios were negative for the $[45°/15°/75°/45°]_{2S}$ tests.[13]

Analysis Predictions Compared to Test Results

As explained previously, an incremental numerical approach was used to obtain the analytical stress-strain-failure predictions. The instantaneous values of the elastic properties were obtained for a particular stress-strain level from the polynomial representation of the stress-strain response of a unidirectional laminate. These values were substituted into the classical lamination theory relationships (equations 1 to 3) for the next increment of the remote load. The resulting stresses were substituted into the respective failure criterion (equations 4 to 6), plywise. When the state of stress in a ply reached or exceeded the interaction surface predicted by the failure criterion, the ply was unloaded either by the reduced stiffness method of Jones[3] or the staggered fracture surface method described earlier. The laminates were assumed to have the same tensile and compressive properties.

The results obtained by the above procedure are shown in Figures 12-14. Figure 12 shows the comparison between analytical predictions and experimental results for the $[0°/\pm30°/0°]_{2S}$ laminate. Excellent correlation is seen up to about 50 ksi (344.8 MPa). At this stress level, failure of the $\pm$ 30° plies was predicted and is indicated by the steeper slope of the stress-strain curve. Thus, analysis and experiment indicated the same trend. After FPF, the analysis predicted higher stresses than were experimentally found. Reasonable correlation between theory and experiment was found for the $[45°/15°/75°/45°]_{2S}$ laminate as is seen in Figure 13. Excellent correlation for the $[90°/\pm60°/90°]_{2S}$ laminate was found as evidenced by Figure 14. On the whole, the analysis predicted larger stiffnesses than were experimentally found. This and the distinct

deviation between analysis and experiment after FPF for the $[0°/\pm30°/0°]_{2S}$ laminate was likely due to omission of the interlaminar shear stresses in the analysis.

Both analytical unloading techniques used gave reasonably the same stress-strain predictions. However, the staggered fracture surface method tended to give more conservative strength predictions than the reduced stiffness method as may be observed on examination of Table 1. This was primarily due to the simplicity of formulation of the former over the latter. The staggered fracture surface method is, in general, computationally easier and a good bit more flexible when modeling laminate behavior beyond FPF. This would be true especially if interlaminar effects were included.

Among the three failure criteria used, Ashkenazi's appears to be the best. It should be noted, however, that equation (4) is only for uniaxial tension. The exponent of the interaction factor for equation (6) used herein was unity. By adjusting this exponent for the various laminates, identical analytical and experimental results could have been obtained. Unfortunately, for the laminates tested herein, this exponent was not a constant and thus the value of unity was used. However, the Puppo and Evensen theory appears to be most promising as it can be used for multi-axial loading, allows for material variations through the interaction factor, and can be used on multi-axial laminates without a plywise analysis. On the whole, good strength predictions were obtained from all three criteria using both unloading techniques.

Conclusions

SEM micrographs have been presented which indicate the types and sizes of inherent flaws encountered in the graphite/epoxy laminates

investigated. Evidence has been presented which indicates that first failure occurred on inner plies. It is thought that this interior failure may account for the audible noise which could be heard at various stages of the loading process. As a result, perhaps accoustic emission might represent an ideal method for identification of failure modes and mechanisms.

Computer conditioned stress-strain data have been presented which indicated that fiber dominated laminated polymer matrix composites appear to have no rate effects whereas polymer matrix dominated laminated composites do show a rate dependence. Some type of transition from one behavior to the other for other laminates does seem to occur. It appears that these laminates first show increase of properties with increased strain rate followed by a decrease of properties for additional increases in strain rate. This is similar to results found previously.[14] Thus, high rates may have deleterious effects on some types of laminates.

Three failure theories have been examined with two methods of unloading. Classical lamination theory in conjunction with these theories has been shown to give reasonably good predictions to actual stress-strain response. Further, the theories also indicated first ply failure on the interior of the $[0°/\pm30°/0°]_{2S}$ laminates with subsequent increased stiffnesses. The three theories and the two unloading schemes have been shown to give reasonable failure strength predictions. It has been suggested that the Puppo-Evensen theory and the staggered failure surface method appear to be the better approach of those attempted.

ACKNOWLEDGEMENTS

The financial support provided for this work by NASA Grant NSG 2038 from the Materials Science Branch of Ames Research Center is gratefully acknowledged. Further, sincere appreciation is extended to D. P. Williams of NASA-Ames for his encouragement and many helpful suggestions. Also, the many helpful discussions with M. F. Kannenin, E. F. Rybicki and W. Griffith of Battelle Columbus Laboratories are acknowledged.

REFERENCES

1. Daniel, I. M.; Rowlands, R.E .; and Whiteside, J. B., "Effects of Material and Stacking Sequence on Behavior of Composite Plates with Holes," Experimental Mechanics, Jan. 1974.

2. Bert, C. W., "Static Testing Techniques for Filament-Wound Composite Materials," Journal of Composite Materials, Jan. 1974.

3. Jones, R. M., Mechanics of Composite Materials, McGraw-Hill Book Company.

4. Ashton, J. E., and Whitney, J. M., "Theory of Laminated Plates," Progress in Materials Science Series, Vol. IV, Technomic Publishing Co., 1970.

5. Sandhu, R. S., "A Survey of Failure Theories of Isotropic and Anisotropic Materials," Technical Report AFFDL-TR-72-71, Air Force Flight Dynamics Laboratory, Wright-Patterson Air Force Base, Ohio.

6. a. Ashkenazi, E. K., "Anisotropy in the Strength of Construction Material," C. M. Kirov Wood Technology Academy, Leningrad, Vol. 31, No. 5, May 1961.

   b. Ashkenazi, E. K., "The Construction of Limiting Surfaces for Biaxial Stressed Condition of Anisotropic Materials," Zavodskaya Laboratoriyz, Vol. 30, No. 2, Leningrad Forestry Academy, February 1964.

   c. Ashkenazi, E. K., "Problems of the Anisotropy of Strength," Mekhanika Polimerov, Vol. 1, No. 2, 1965.

7. Hill, R., "A Theory of the Yielding and Plastic Flow of Anisotropic Metals," Proceedings of the Royal Society, Series A, Vol. 193, 1948.

8. Puppo, A. H., and Evensen, H. A., "Strength of Anisotropic Materials Under Combined Stresses," AIAA/ASME 12th Structures, Structural Dynamics and Materials Conference, Anaheim, California, April 19-21.

9. Cole, B. W., and Pipes, R. B., "Filamentary Composite Laminates Subjected to Biaxial Stress Fields," Technical Report AFFDL-TR-73-115, Air Force Flight Dynamics Laboratory, Wright-Patterson Air Force Base, Ohio.

10. Tsai, S. W. and Hahn, H. T., "Failure Analysis of Composite Materials," Inelastic Behavior of Composite Materials, (C. T. Herakovich, ed.), ASME, New York, 1975.

11. Petit, P. H., and Waddoups, E. M., "A Method of Predicting the Non-linear Behavior of Laminated Composites," Journal of Composite Materials, January 1969.

12. Sandhu, R. S., "Ultimate Strength Analysis of Symmetric Laminates," Technical Report AFFDL-TR-73-137, Air Force Flight Dynamics Laboratory, Wright-Patterson Air Force Base, Ohio.

13. Brinson, H. F., and Yeow, Y. T., "An Investigation of the Failure and Fracture Behavior of Graphite/Epoxy Laminates," VPI-E-75-23, V.P.I. & S.U. Report, Sept. 1975.

14. Heller, R. A.; Brinson, H. F.; Thakker, A. B., "Environmental Effects on Fiber-Reinforced Composites," Polymer Engineering and Science, Vol. 15, No. 11, Nov. 1975.

Figure Captions

Figure 1. Sideview of $[0°/\pm30°/0°]_S$ Laminate.
a) At First Ply Failure
b) At Final Fracture

Figure 2. Inherent Flaws in $[0]_{8S}$ Graphite/Epoxy Laminates.
a) Left; 300X b) Right; 600X

Figure 3. Fracture Planes in Unnotched Laminates.
a) Upper; $[0]_{8S}$ specimen showing axial splitting.
b) Lower; $[0/\pm30/0]_{2S}$ specimen showing delamination.

Figure 4. SEM Micrographs of $[0]_{8S}$ Fracture Surface.
a) Left; 35X b) Right; 2000X

Figure 5. Load-Time and Strain-Time Trace for $[90°/\pm60°/90°]_{2S}$ Specimen.

Figure 6. Stress-Strain Curves of $[0°]_{8S}$ Laminate.

Figure 7. Stress-Strain Curves of $[45°]_{8S}$ Laminate.

Figure 8. Stress-Strain Curves of $[90°]_{8S}$ Laminate.

Figure 9. Stress-Strain Curves of $[0°/\pm30°/0°]_{2S}$ Laminate.

Figure 10. Stress-Strain Curves of $[45°/15°/75°/45°]_{2S}$ Laminate.

Figure 11. Stress-Strain Curves of $[90°/\pm60°/90°]_{2S}$ Laminate.

Figure 12. Comparison of Experimental Results with Analytical Predictions of $[0°/\pm30°/0°]_{2S}$ Laminate.

Figure 13. Comparison of Experimental Results with Analytical Predictions of $[45°/15°/75°/45°]_{2S}$ Laminate.

Figure 14. Comparison of Experimental Results with Analytical Predictions of $[90°/\pm60°/90°]_{2S}$ Laminate.

Table 1. Predicted Failure Strength, Normalized with Respect to the Experimental Load.

Laminate Orientation	Ashkenazi	Hill	Puppo-Evensen
	Staggered Failure Surface Method		
$[0°/\pm30°/0°]_{2S}$	0.979	0.900	1.021
$[45°/15°/75°/45°]_{2S}$	0.912	0.879	0.889
$[90°/\pm60°/90°]_{2S}$	0.636	0.648	0.587
	Reduced Stiffness Method		
$[0°/\pm30°/0°]_{2S}$	0.971	0.965	0.968
$[45°/15°/75°/45°]_{2S}$	1.002	1.168	1.054
$[90°/\pm60°/90°]_{2S}$	0.827	0.786	0.864

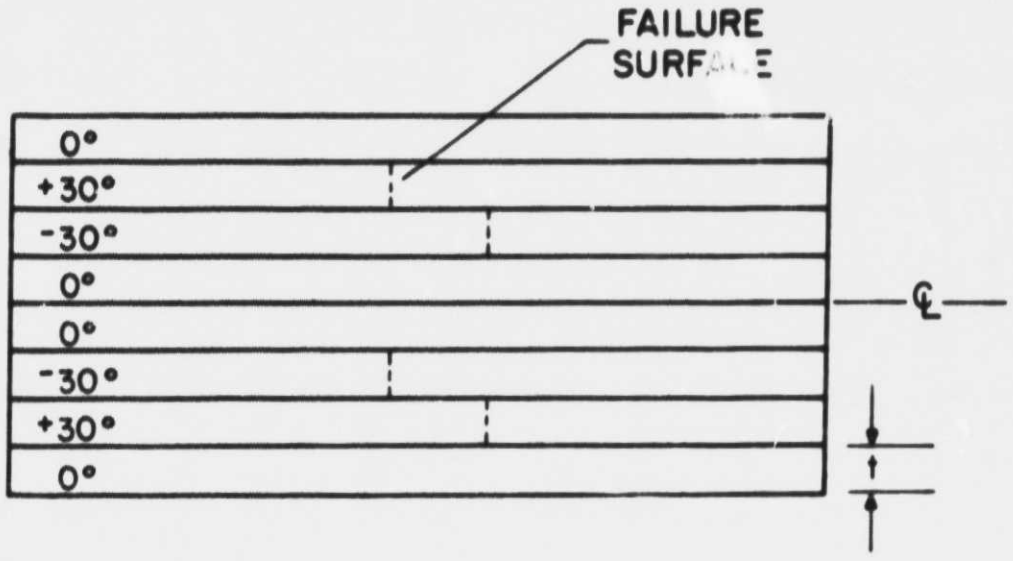

a) At First Ply Failure

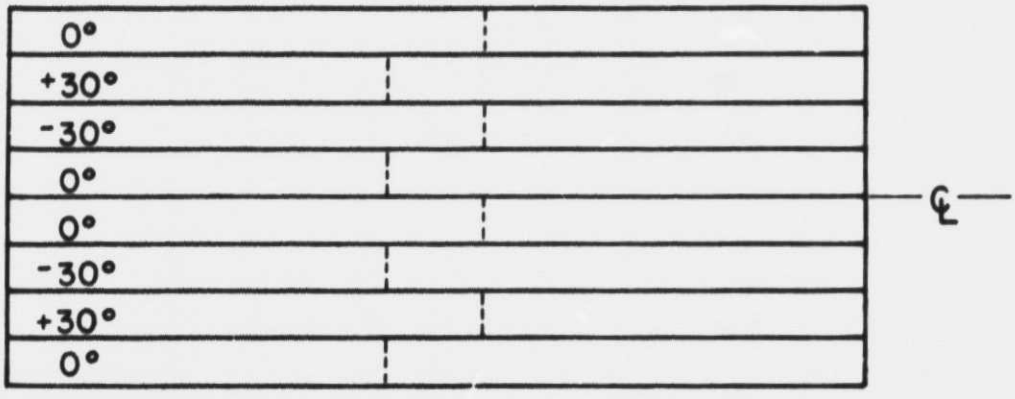

b) At Final Fracture

Fig. 1. Sideview of $[0°/+30°/0°]_S$ Laminate.

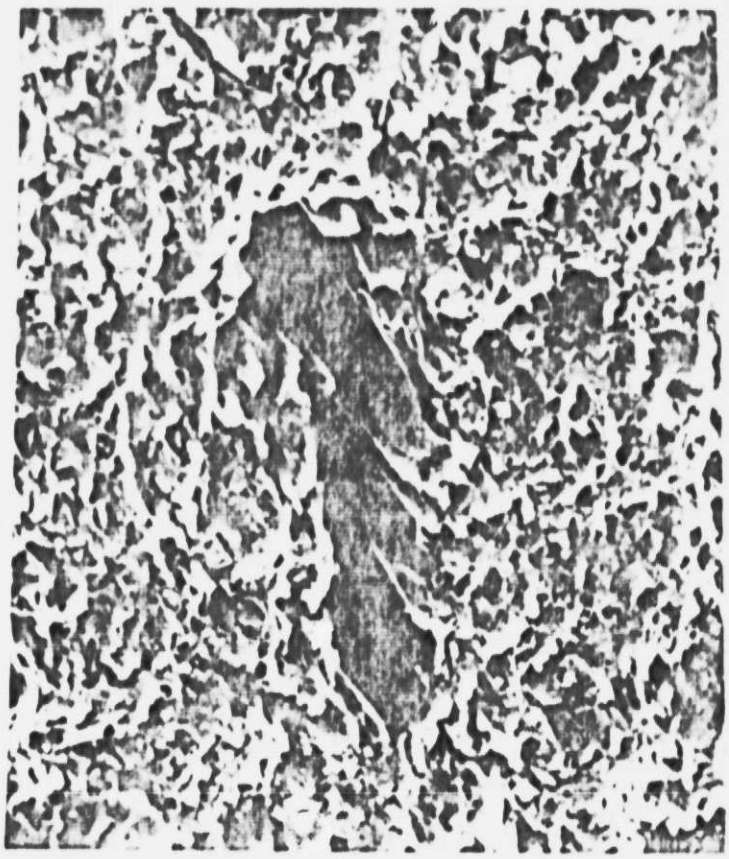

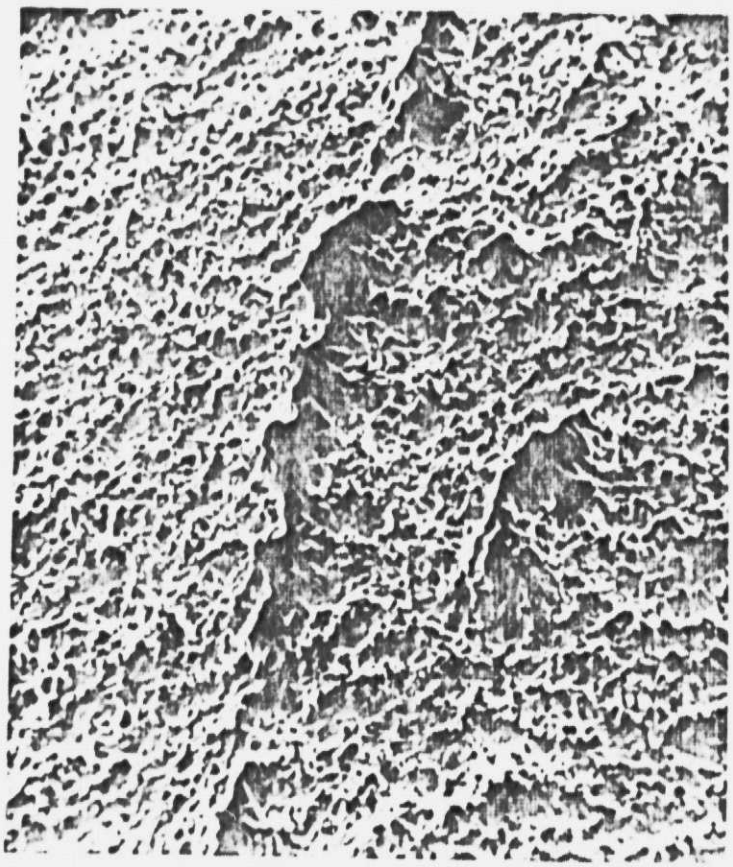

Figure 2. Inherent Flaws in [0]8s Graphite/Epoxy Laminates.
a) Left: 30X b) Right: 60X

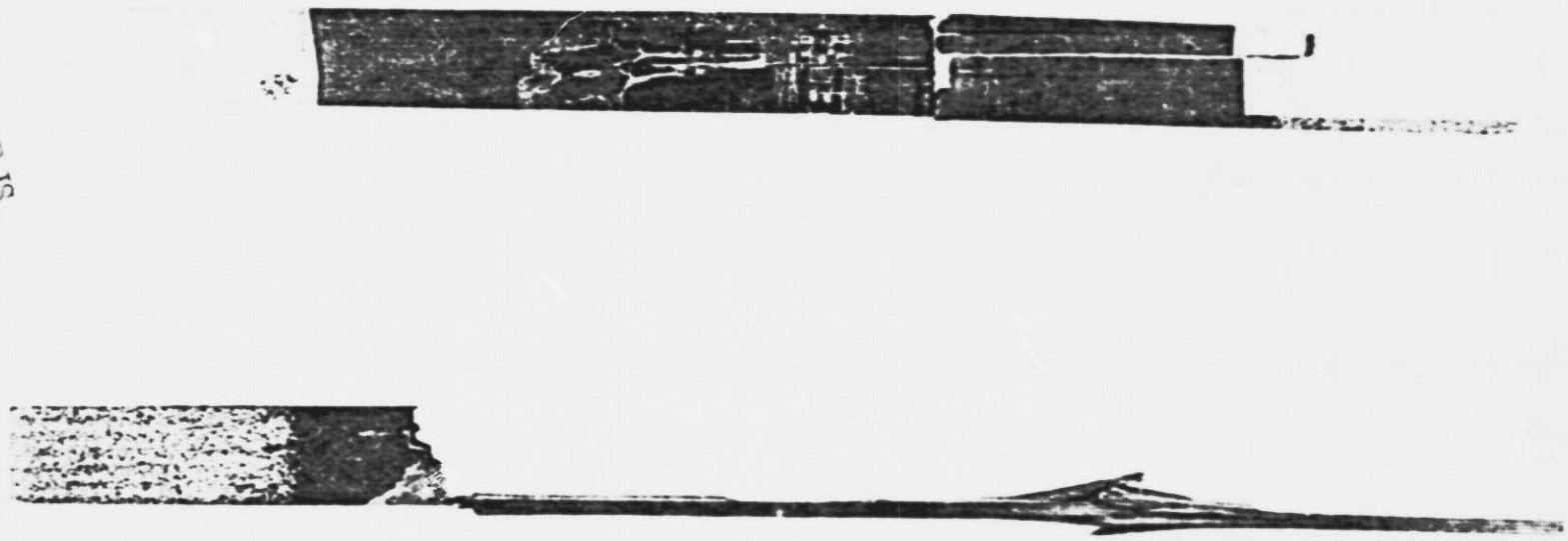

Figure 3. Fracture Planes in Unnotched Laminates.
a) Upper; $[0]_{8S}$ specimen showing axial splitting.
b) Lower; $[0/\cdot 30/0]_{2S}$ specimen showing delamination.

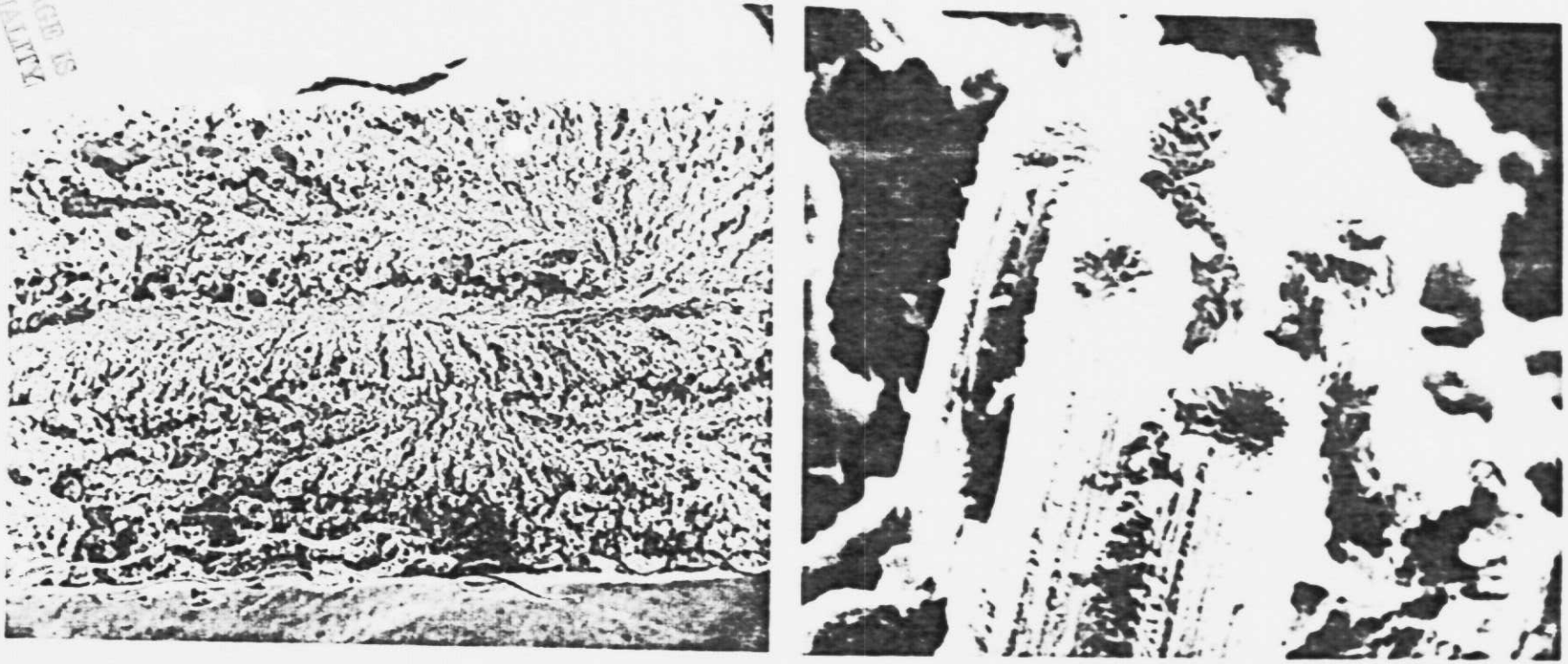

Figure 4. SEM Micrographs of $[0]_{8S}$ Fracture Surface.
a) Left: 35X b) Right: 2000X

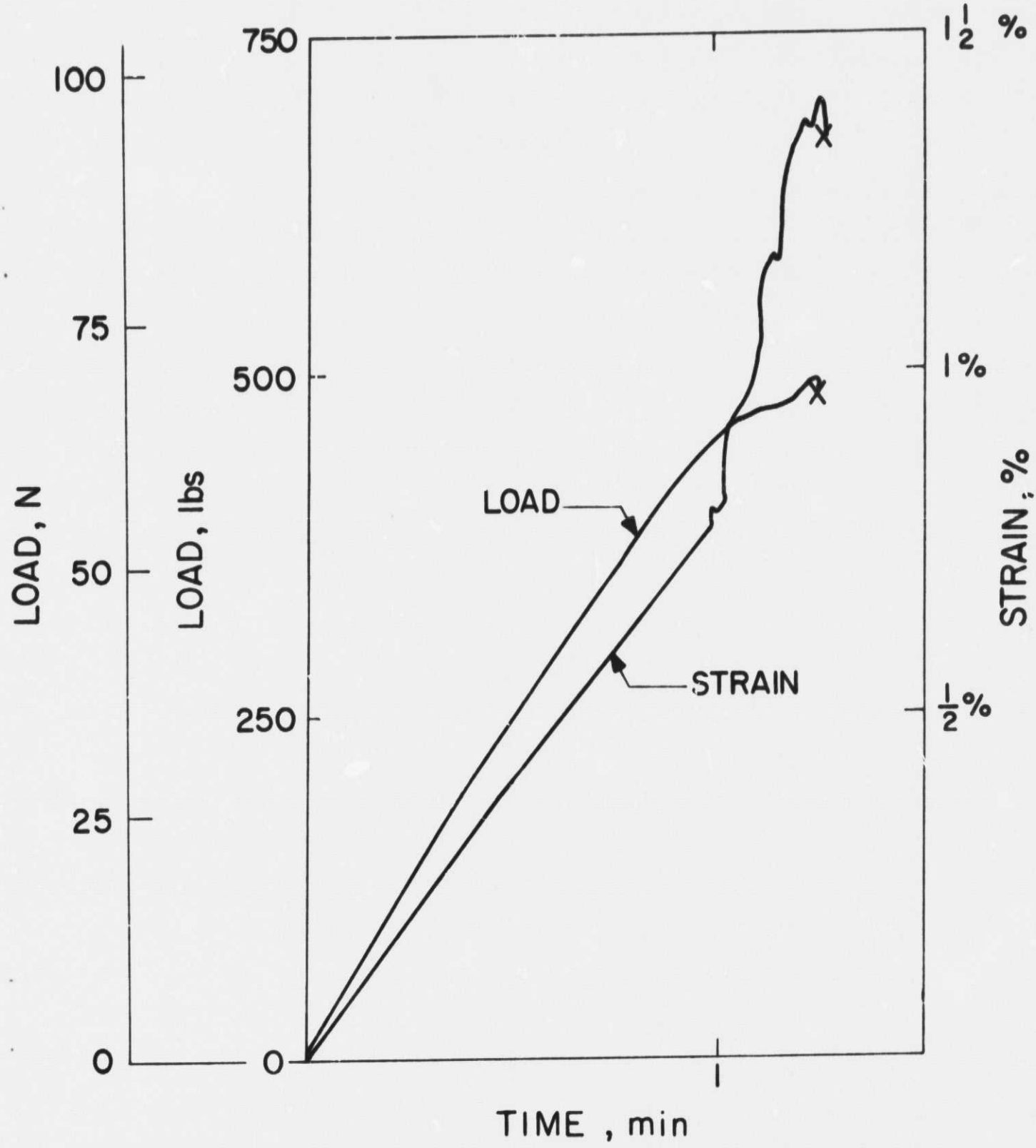

Figure 5. Load-Time and Strain-Time Trace for $[90°/\pm 60°/90°]_{2S}$ Specimen.

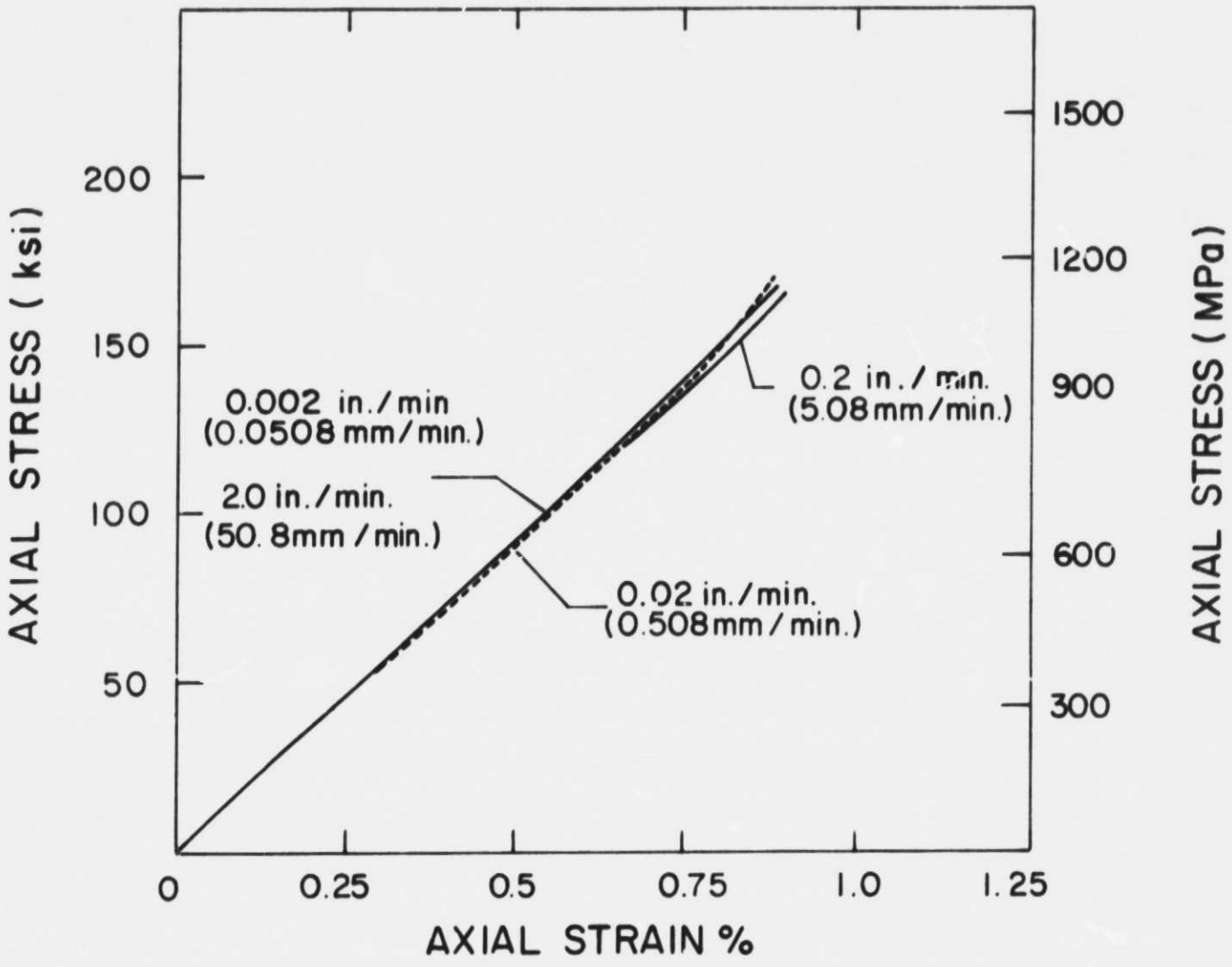

Figure 6. Stress-Strain Curves of $[0°]_{8S}$ Laminate.

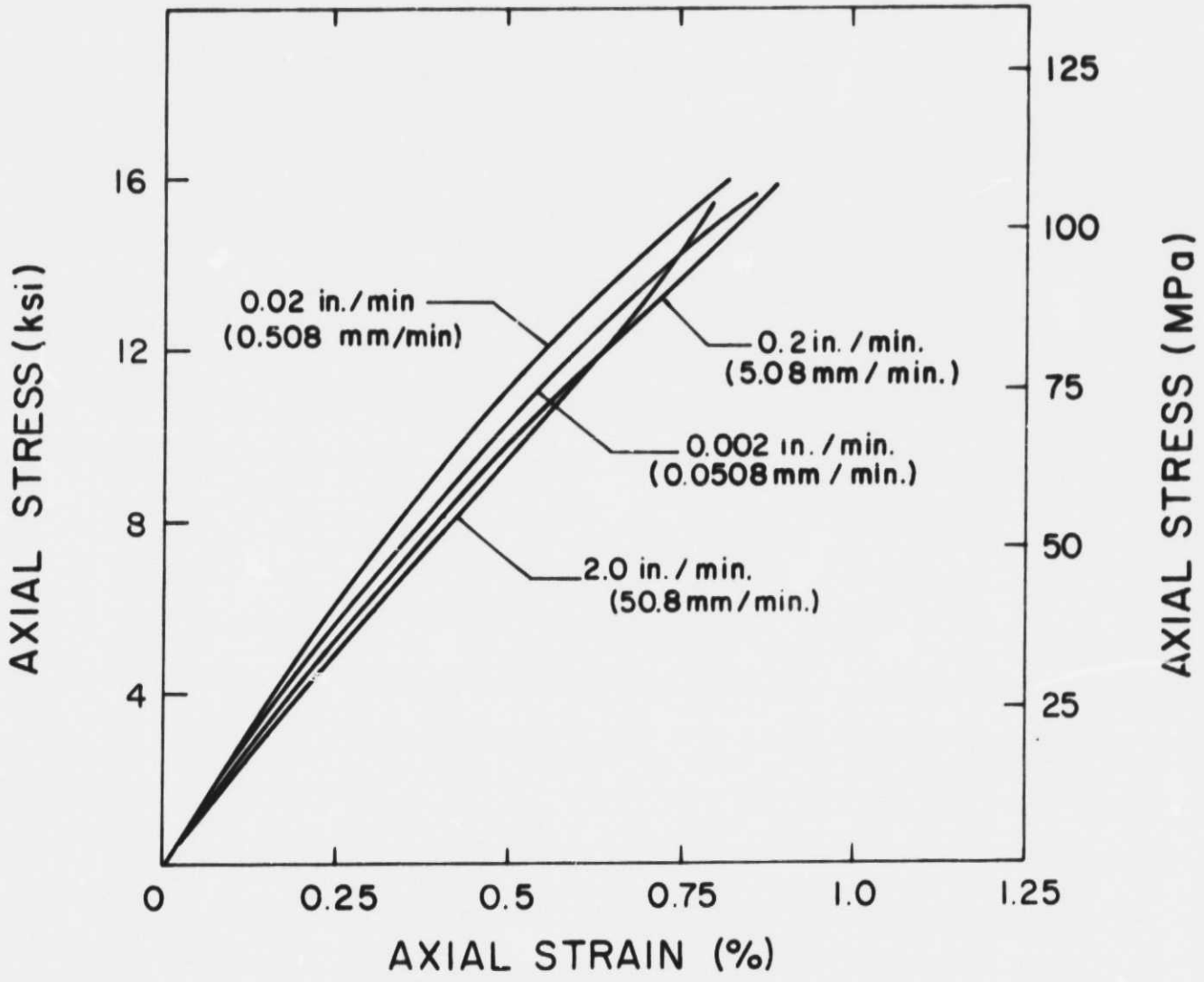

Figure 7. Stress-Strain Curves of $[45°]_{8S}$ Laminate.

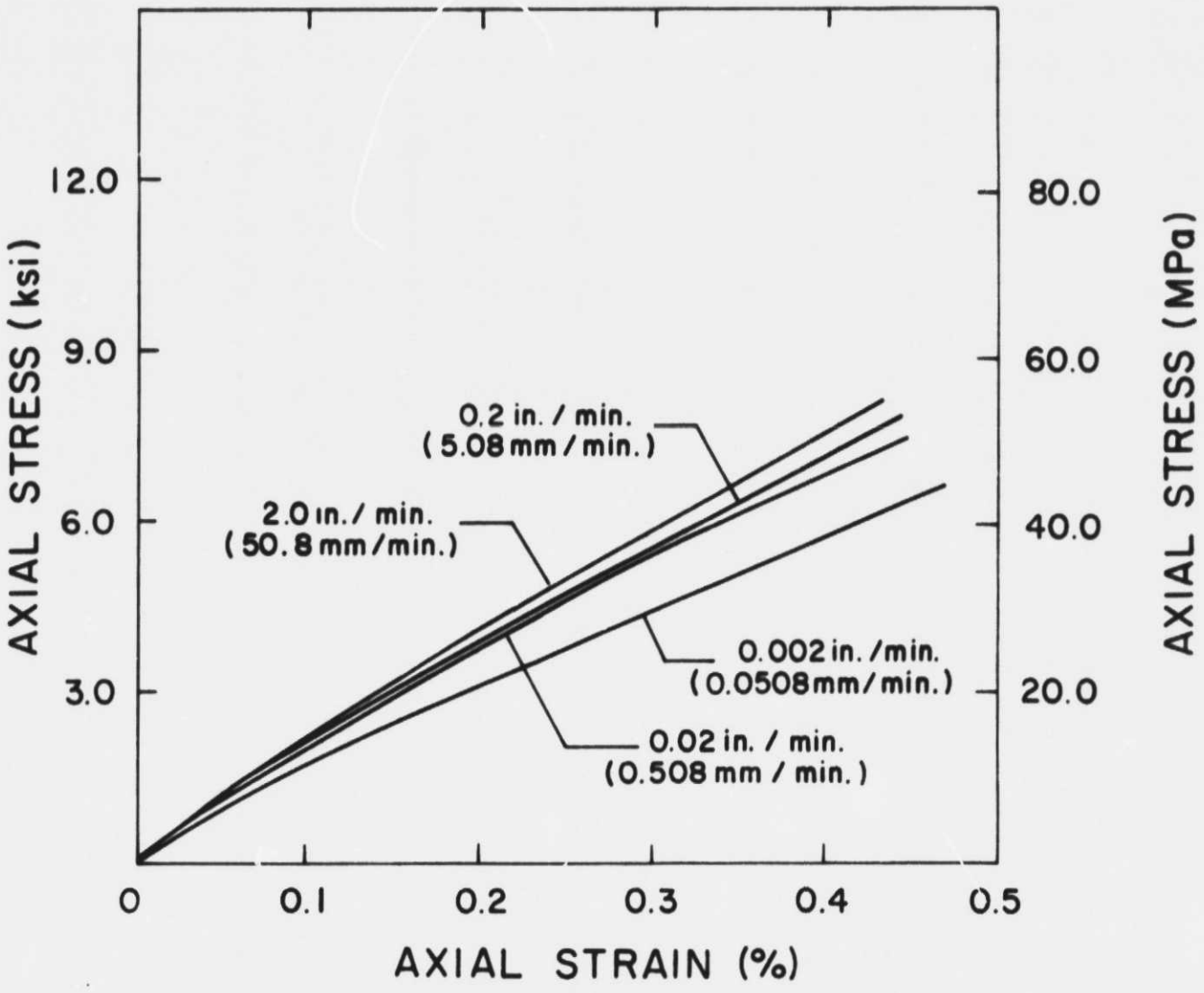

Figure 8. Stress-Strain Curves of $[90°]_{8S}$ Laminate.

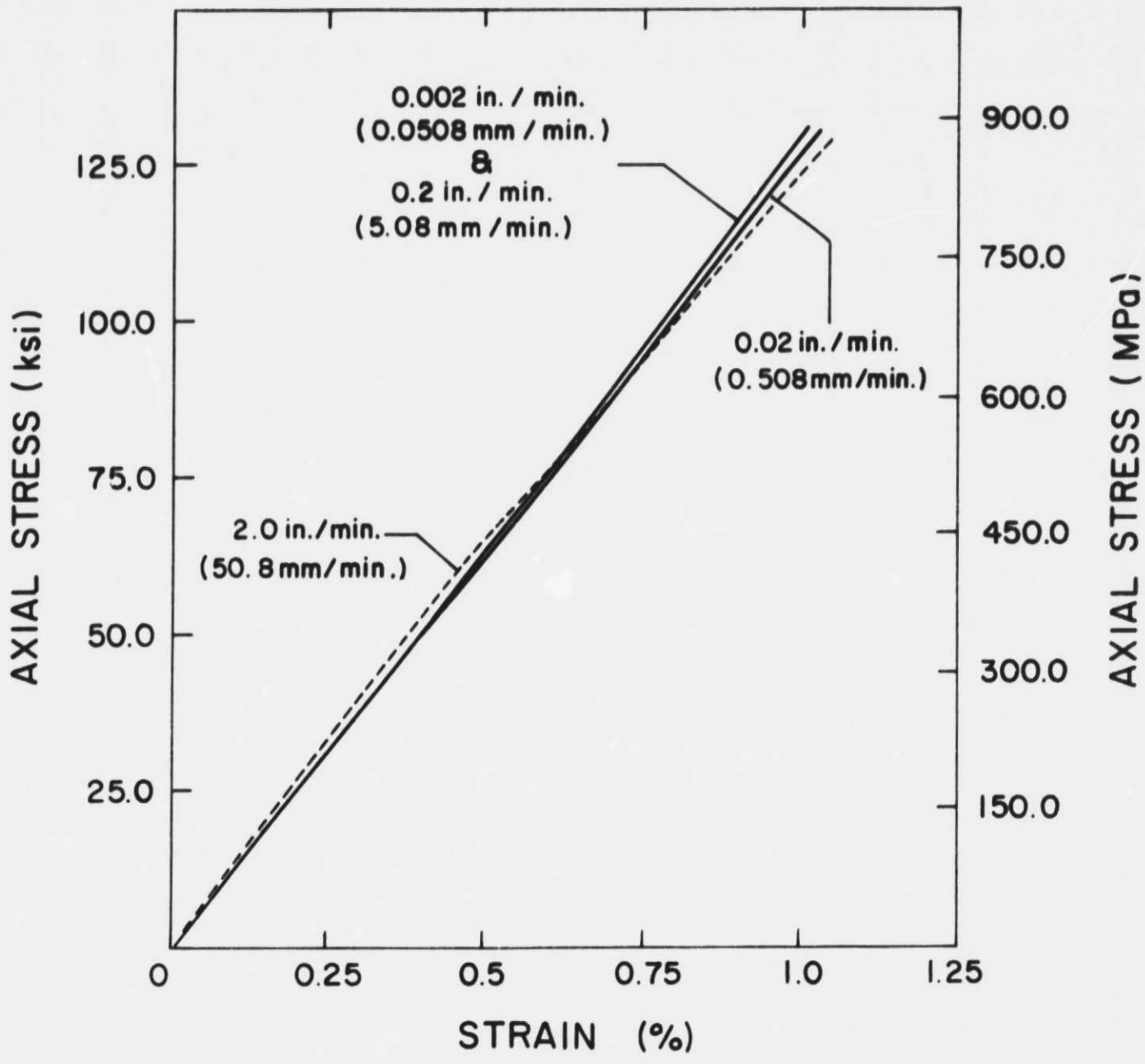

Figure 9. Stress-Strain Curves of $[0°/\pm30°/0°]_{2S}$ Laminate.

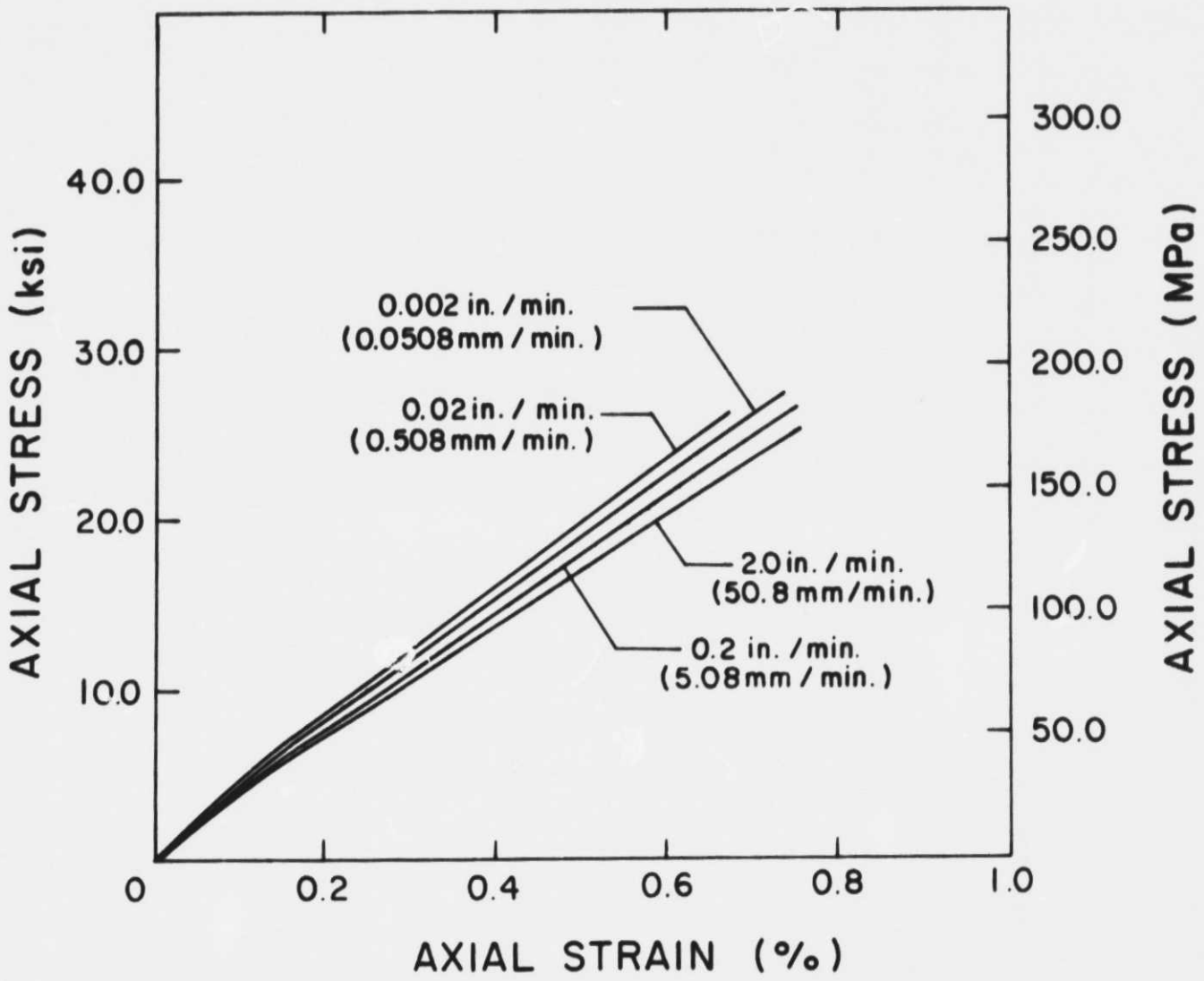

Figure 10. Stress-Strain Curves of $[45°/15°/75°/45°]_{2S}$ Laminate.

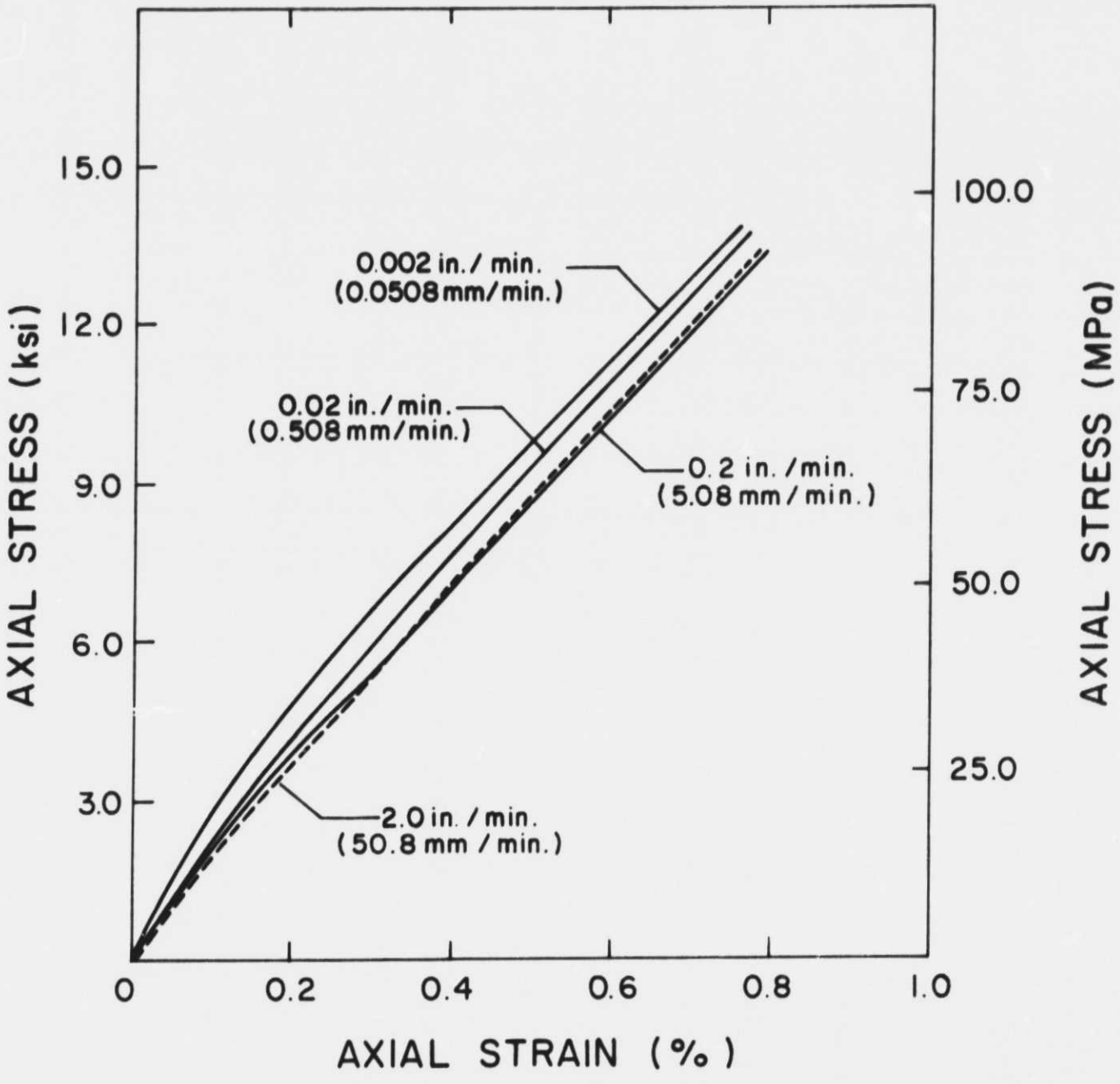

Figure 11. Stress-Strain Curves of $[90°/\pm60°/90°]_{2S}$ Laminate.

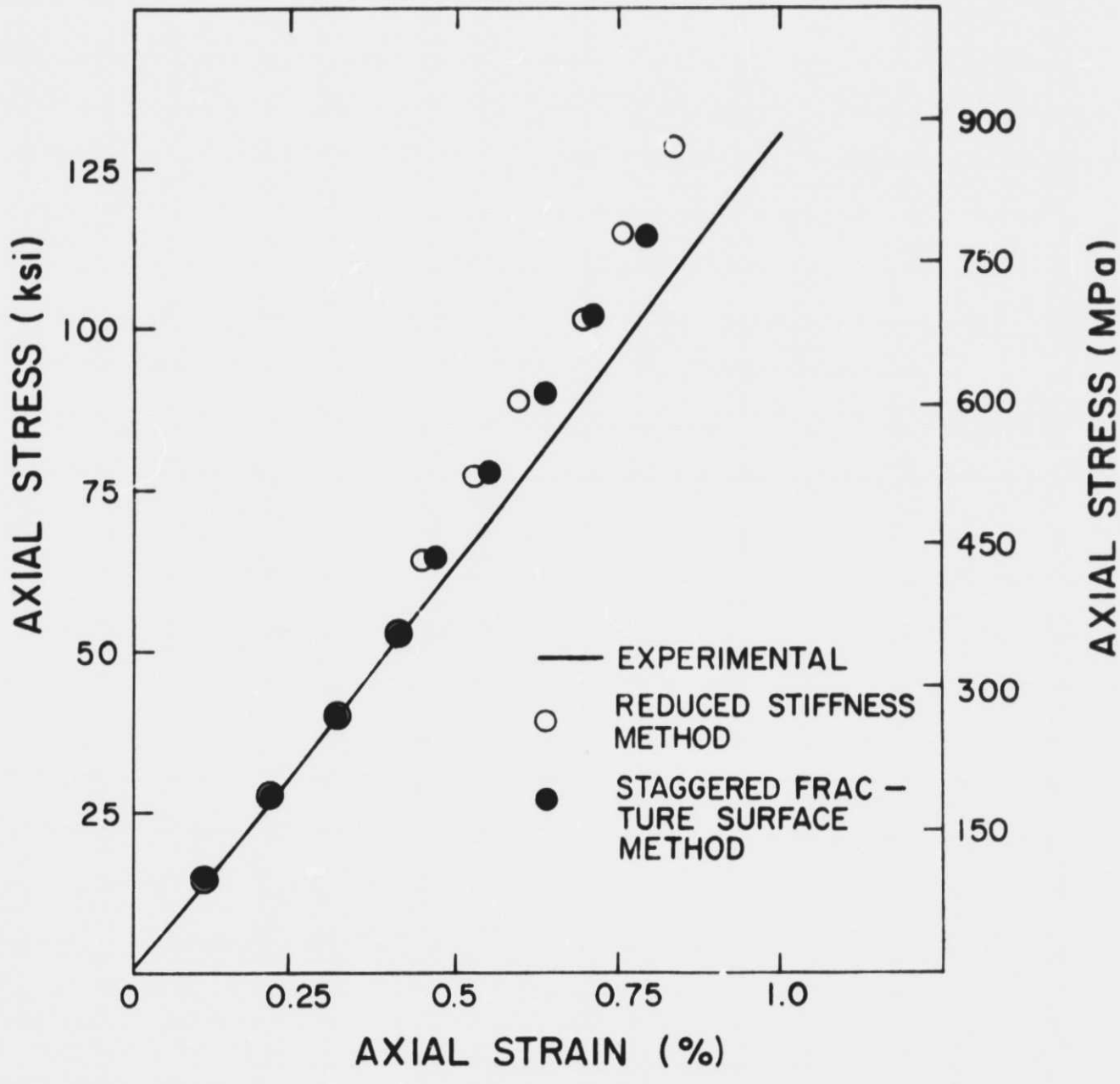

Figure 12. Comparison of Experimental Results with Analytical Predictions of $[0°/\pm30°/0°]_{2S}$ Laminate.

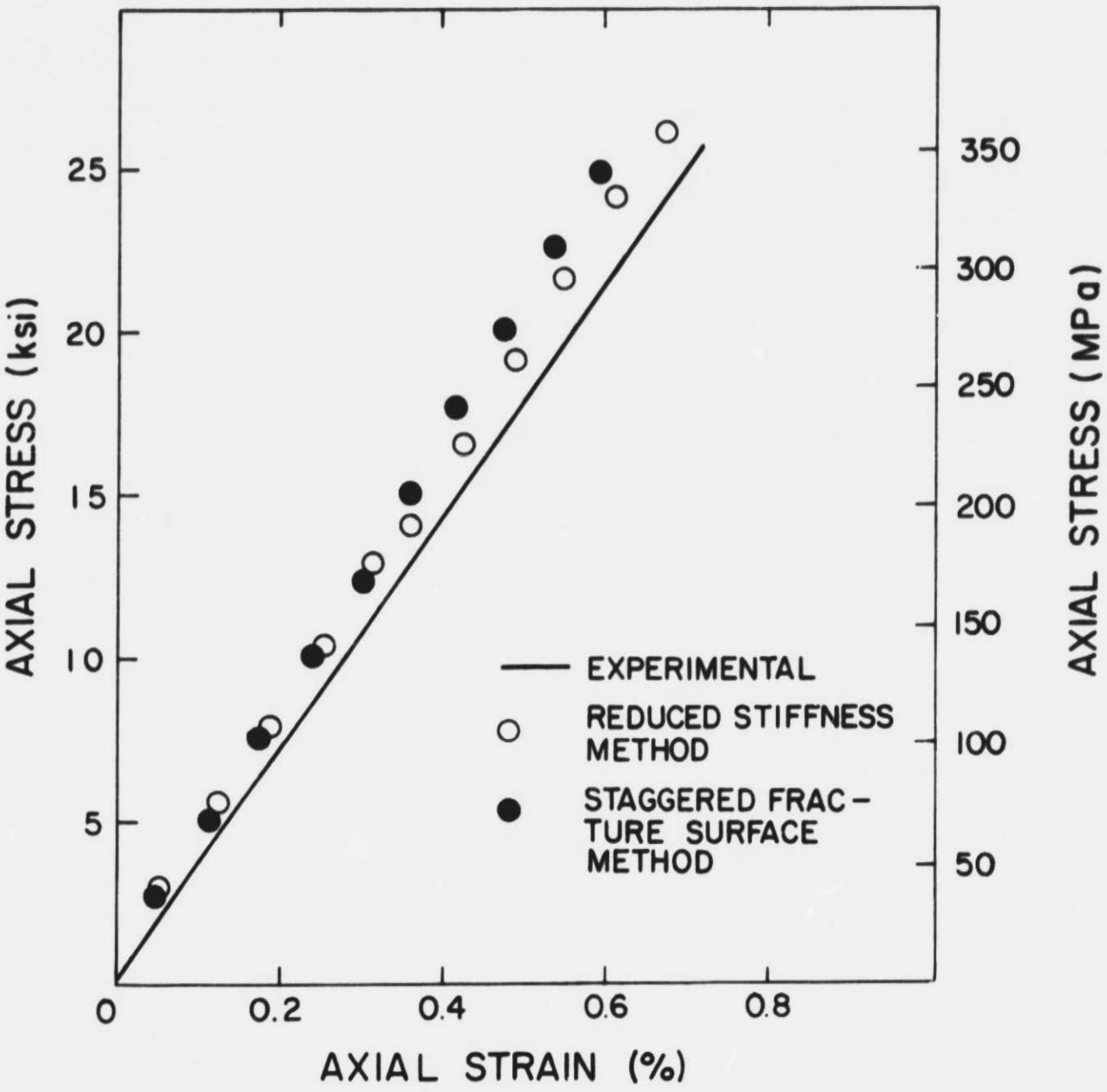

Figure 13. Comparison of Experimental Results with Analytical Predictions of $[45°/15°/75°/45°]_{2S}$ Laminate.

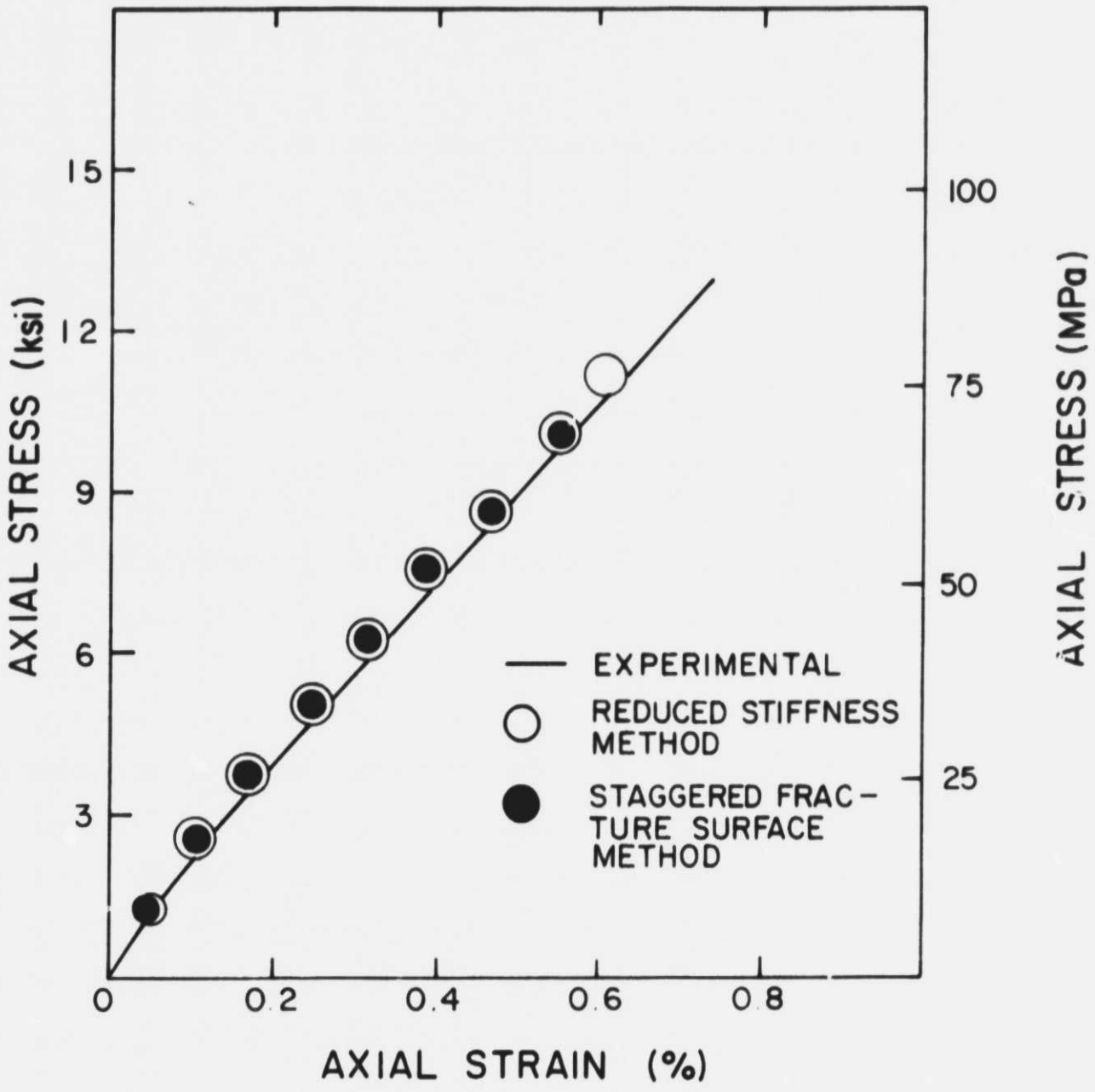

Figure 14. Comparison of Experimental Results with Analytical Predictions of $[90°/\pm 60°/90°]_{2S}$ Laminate.